Exciton Interactions and Femtosecond Relaxation in Chlorophyll *a*−Water and Chlorophyll *a*−Dioxane Aggregates

J. Linnanto,* V. M. Helenius, J. A. I. Oksanen, T. Peltola, J.-L. Garaud, and J. E. I. Korppi-Tommola

Department of Chemistry, University of Jyväskylä, P.O. Box 35, FIN-40351 Jyväskylä, Finland

Received: September 2, 1997; In Final Form: April 10, 1998

Chlorophyll *a* (Chl *a*) in hydrocarbon solution with a small amount of dioxane or water shows red-shifted absorption bands at 686 nm and at 700 nm (dioxane) and at 745 nm (water), indicative of self-organized aggregate structures in solution. To study the relationship between the structure and spectral properties of the aggregates, several one-dimensional model structures of Chl *a*−dioxane and Chl *a*−water aggregates were computed by the molecular mechanics method. Three overall structures ranging from stick to a ring shape were energetically favored for the dioxane system. All these structures contain structural heterogeneity that consists of repeating dimers that further form tetramer substructures. For the Chl *a*−water system a one-dimensional homogenous helical structure was obtained. By using the model structures, the transition energies and fluorescence excitation polarizations were computed. Exciton theory with dipole−dipole interaction approximation and semiempirical quantum mechanical CI calculations were used. Excitonic splittings of the aggregate transition energies were calculated by diagonalizing 10 × 10 interaction matrixes. For the Chl *a*−dioxane dimers, trimers, and tetramers the exciton theory with dipole−dipole interaction approximation produced blue-shifted exciton transitions of the computed structures, while the semiempirical calculation gave red-shifted transitions for all these species, the tetramer shifts being closest to the experimental shifts. The quantum chemical calculations of the two tetramers appearing in the computed one-dimensional model structure predict the quartet structure of the absorption spectrum. The calculations also produce fluorescence excitation polarizations that are very similar to the values observed at low temperatures for the Chl *a*−dioxane aggregate. In the case of the Chl *a*−water aggregate both dipole approximation and semiempirical exciton shifts were only one-half of the observed spectral shift. It is suggested that the remainder is due to the environmental effects not included in the calculations, like two-dimensional chromophore−chromophore interactions and solvent effects in the Chl *a*−water aggregate. Calculations on the Chl *a*−water and Chl *a*-dioxane model aggregates demonstrate that at close chromophore−chromophore distances the dipole−dipole approximation and the semiempirical calculation give very different results. The results from the model calculations are compared with available spectral data of each aggregate together with new femtosecond results for the Chl *a*−water aggregate. In one-color absorption recovery experiments the Chl *a*−water aggregate shows an obvious wavelength dependence of electric relaxation. The decay has a strong femtosecond component (about 300 fs) in the blue side of the Q_y band that is not present in the red side. No rise time could be observed when the Q_y band was pumped in the blue side and probed in the red side with 350 fs time resolution. Our results suggest that thermalization of the excitation energy of the Chl *a*−water aggregate takes place in less than 350 fs.

Introduction

Monomeric Chl *a* solutions may be prepared in hydrocarbons by adding in very small amounts of polar solvent molecules such as pyridine or acetone. It is well-known that these polar molecules bind to the central magnesium atom of Chl *a*, producing pigment−solvent complexes.[1,2] Solvent coordination prevents Chl *a* molecules from forming self-aggregates. In aliphatic hydrocarbons where coordination of the solvent to the central magnesium atom does not take place, Chl *a* forms self-aggregates via coordination of the C-13[1] oxo group to the central magnesium atom of the next Chl *a*.[1,3] These aggregates are weakly bound (small spectral shift) and small in size.[4] Bacteriochlorophylls *c* and *d* also form self-aggregates, where the hydroxyl groups of the pigments provide a strong binding site. These aggregates show a large red shift of the Q_y absorption band, they are large in size, and they have been proposed to have a well-defined, most probably a rodlike structure.[5] If a small amount of bifunctional linker molecule is dissolved in a solution of chlorophyll or bacteriochlorophyll in hydrocarbon, aggregation takes place as well.[6] The size and the structure of the aggregate and its spectroscopic properties depend strongly on the linker molecule, concentration, and temperature. By varying the linker molecule it is possible to generate various structures of aggregates and to study the basic photophysical mechanisms governing the excitonic coupling and energy-transfer properties of these species.

Here we report results on two Chl *a* aggregates where dioxane and water serve as bridging molecules. Excitonic and energy-transfer properties of the aggregates were studied by absorption, fluorescence, and femtosecond transient absorption spectroscopy. Molecular mechanics computer simulation was used in modeling of the structures of the aggregates and exciton theory,

S1089-5639(97)02852-1 CCC: $15.00
Published on Web 05/19/1998

and quantum mechanical calculations were used to estimate the transition energies.[7]

Molecular exciton theory has frequently been applied to Chl aggregates and photosynthetic pigment protein complexes with the expectation that insight into the relationship between the structure and spectral properties can be obtained.[8−10] Chow *et al.* and Shipman *et al.*[9] have investigated a one-dimensional chain of Chl *a*−water adducts in a geometry derived from the crystal structure of ethyl chlorophyllide *a* dihydrate. By using a dipole−dipole interaction in an exciton calculation, they were able to show that the red shift of the Q_y absorption increases with the size of the aggregate.[8] Our exciton calculations of the Chl *a*−water adduct are in agreement with the earlier results. The main difference between the semiempirical CI calculation and the exciton calculation of the Chl *a*−water adduct is that the former method describes the red shift slightly better than the latter, yet only half of the experimental shift is predicted by any available calculation. The difference between the exciton and semiempirical calculations is more striking in the Chl *a*−dioxane aggregate. The semiempirical CI calculations on the one-dimensional Chl *a*−dioxane model structures give very different spectral properties from what is obtained by the exciton theory with dipole−dipole interaction for the same structure. The result is somewhat surprising because the dioxane as a linker molecule keeps, according to the calculation, the distance between the adjacent porphyrins at about 7 Å. Therefore one could expect that the dipole−dipole interaction would work in this case even better than in the case of Chl *a*−water adduct, where the distance between the porphyrin planes is only 3.3 Å. Our results demonstrate that the semiempirical calculations and the dipole−dipole approximation for the same structures give different results. This is not surprising since the effects from the orbital overlap of the interacting chromophores and inclusion of the environmental effects, such as the effect of the linker molecule, are only included in the quantum mechanical calculation.

We believe that study of aggregates of the basic photosynthetic chromophores Chl *a*, Chl *b*, Bchl *a*, and Bchl *c* present in plants and bacteria, respectively, helps the understanding of excitonic interactions and energy transfer between the pigments. Our solutions are free from the effects of detergents, and linker molecules are present only at very small quantities. It is hoped that results from such chemically well-defined systems are useful in the study of structure−spectrum relationship and energy-transfer properties of in vivo light-harvesting systems of plants and bacteria.[11,12]

Experimental and Computational Methods

The details of measuring the absorption, fluorescence, CD, and LD spectra are given in ref 13. A site-selective fluorescence experiment of Chl *a*−water adduct in 3-methylpentane was done by using an argon ion laser pumped titanium−sapphire CW laser (Coherent Inc.) as an excitation source and a Chromex 500IS imaging spectrograph together with Cromspec CCD detector. The sample was in a 10 mm quartz cell. OD at the absorption maximum (745 nm) was about 0.2. Sample preparation is described in detail in ref 13.

The femtosecond laser spectrometer used in this work consists of a seeder laser (Coherent Mira 900 titanium−sapphire laser) pumped by a CW argon ion laser (Coherent Innova 400) at about 13 W for all lines. Mira 900 produces from 80 to 200 fs pulses at a repetition rate of 76 MHz. The stretched seeder pulses of 100−300 ps duration **(**Quantronix model 4820 Stretcher/Compressor) were fed into a regenerative amplifier (Quantronix 4800 Series Ti:sapphire RGA) pumped at 1 kHz by the SHG output of a Q-switched Quantronix 527 Nd:YLF laser. The amplified picosecond pulses were then compressed back to 200 fs of duration. The amplified pulse energy was typically 300 μJ at 745 nm and about 550 μJ at 800 nm. The wavelength of the system may be tuned from 730 to 900 nm. For recording pump and probe signals both a lock-in amplifier and a three-channel diode detection data acquisition system may be used. In the diode detection system the probe beam is split into two beams of equal intensity and the excitation beam is chopped at 40 Hz. Computer software monitors whether the chopper is open or closed and disregards partially blocked pulses. The difference of the logarithms of the ratios of the sample and reference probe pulse intensities with chopper open and chopper closed positions is computed to produce the pump pulse induced optical density change in the sample. Normally signal averaging includes 1000 shots for a single data point, and one measurement contains some 600 data points. The system can detect absorbance changes of about 0.2 mOD around 750 nm.

The monomer structures of Chl *a* and dioxane were fully optimized at the PM3 level[14] on a Silicon Graphics PERSONAL IRIS 4D/35 TG+ workstation by using the SPARTAN (Wavefunction Inc.) software.[15] The geometry optimizations were then continued on a Cray XMP supercomputer at the National Center for Scientific Computing in Espoo, Finland, at the PM3-CI level by using the MOPAC software package.[16] Optimized monomer geometry was used to compute structures of the molecular aggregates with the QUANTA (release 3.2) software on a Silicon Graphics PERSONAL IRIS 4D/35 TG+ workstation. The standard parameters of QUANTA were used with the exception that the bond length between the porphyrin ring nitrogens and the magnesium atom was set to 2.086 Å. This value was taken from X-ray structure of ethyl chlorophyllide *a*.[8] The aggregate structures were minimized by using a molecular mechanics method with the CHARMm force field and Newton Raphson optimization.[17] Single-point ZINDO/S[18−20] semiempirical CI calculations of the dimer, timer, and tetramer aggregates were performed by using HyperChem software[21] running on a 133 MHz Pentium PC with 128 MB of memory.

Theory

Calculation of Excitonic Energies. To make use of the computed aggregate structures, excitonic energies were evaluated for each structure.[7] We describe the method shortly. Consider an assembly of N molecules (not necessarily identical) that form an aggregate. Assume that the Born−Oppenheimer approximation is valid for the aggregate. Let us suppose that the Hamiltonian of the aggregated system is of the form

$$\hat{H} = \sum_{i=1}^{N} \hat{H}_i + \sum_{i<j}^{N} \hat{H}_{ij} + \sum_{i=1}^{N} \hat{V}_i \qquad (1)$$

where $\hat{H}_i$ involves electrons and nuclei on the ith molecule, $\hat{H}_{ij}$ contains electron−electron, nuclear−electron, and nuclear−nuclear interaction terms between molecules i and j, and $\hat{V}_i$ contains phonon and exciton−phonon interaction terms on the ith molecule.

In the molecular aggregate there is usually little overlap between the electronic wave functions of the neighboring molecules. To simplify calculations, we have neglected the exchange effects. If the electronic wave function for the kth electronic state of the jth molecule in the aggregate is represented by the ket vector $|\phi_j^k\rangle$ then in the zeroth approximation, the

ground electronic state ($k = 0$) wave function of a molecular aggregate has the form

$$|\Psi_g\rangle = \prod_{j=1}^{N} |\phi_j^0\rangle \tag{2}$$

where the ket vectors $|\phi_j^k\rangle$ ($k = 0$) are orthonormal. When the perturbation term $\hat{V}_i$ is neglected, the approximate energy of the ground state of the molecular aggregate is

$$E_g = \frac{\langle\Psi_g|\hat{H}|\Psi_g\rangle}{\langle\Psi_g|\Psi_g\rangle} = \langle\Psi_g|\hat{H}|\Psi_g\rangle = \sum_{i=1}^{N} E_i^0 \langle\Psi_g|\Psi_g\rangle + \sum_{i<j}^{N} \langle\Psi_g|\hat{H}_{ij}|\Psi_g\rangle$$

$$= \sum_{i=1}^{N} E_i^0 + \sum_{i<j}^{N} \langle\phi_i^0\phi_j^0|\hat{H}_{ij}|\phi_i^0\phi_j^0\rangle \tag{3}$$

When the *i*th molecule is excited to its first excited state and all other molecules in the aggregate are in their ground states, the excited state of the molecular aggregate can be described by the wave fimction

$$|\Psi^i\rangle = [\prod_{j=1}^{i-1} |\phi_j^0\rangle]|\phi_i^1\rangle[\prod_{j=i+1}^{N} |\phi_j^0\rangle] \tag{4}$$

The *N*-dimensional energy matrix **H** may be evaluated and the matrix elements calculated from

$$H_{ii} = \langle\Psi^i|\hat{H}|\Psi^i\rangle = \sum_{j\neq i}^{N} E_j^0 + E_i^1 + \sum_{\substack{j<k \\ j\neq i\neq k}}^{N} \langle\phi_j^0\phi_k^0|\hat{H}_{jk}|\phi_j^0\phi_k^0\rangle + \sum_{j\neq i}^{N} \langle\phi_i^1\phi_j^0|\hat{H}_{ij}|\phi_i^1\phi_j^0\rangle \tag{5}$$

$$H_{ij} = H_{ji} = \langle\Psi^i|\hat{H}|\Psi^j\rangle = \langle\phi_i^0\phi_j^1|\hat{H}_{ij}|\phi_i^1\phi_j^0\rangle \tag{6}$$

The **H** matrix is diagonalized to get the eigenvalues and eigenvectors. Before diagonalizing, we modify the matrix **H** into matrix **H′**

$$(H')_{NN} = (H)_{NN} - E_g \cdot (I)_{NN} \tag{7}$$

It is well-known that vectors $\vec{v} = (v_1, ..., v_n)$ are eigenvectors of the unit matrix $I = (I)_{nn}$, and hence **H** and **H′** have the same eigenvectors, so they describe the same physical system. Now the matrix elements may be written in the form

$$H'_{ii} = E_i^1 - E_i^0 - \sum_{j\neq i}^{N} \langle\phi_i^0\phi_j^0|\hat{H}_{ij}|\phi_i^0\phi_j^0\rangle + \sum_{j\neq i}^{N} \langle\phi_i^1\phi_j^0|\hat{H}_{ij}|\phi_i^1\phi_j^0\rangle \tag{8}$$

$$H'_{ij} = H'_{ji} = \langle\phi_i^0\phi_j^1|\hat{H}_{ij}|\phi_i^1\phi_j^0\rangle \tag{9}$$

When the environmental shift is neglected (the sum terms in the eq 8),[22] then the diagonal matrix elements contain only transition energies of the isolated monomers and off-diagonal matrix elements are transition density−transition density interaction energies. These interaction energies may be calculated using the well-known dipole−dipole interaction Hamiltonian:

$$\hat{H}_{ij} = \frac{1}{4\pi\epsilon_0}\left[\frac{\vec{\mu}_i \cdot \vec{\mu}_j}{R_{ij}^3} - \frac{3(\vec{\mu}_i \cdot \vec{R}_{ij})(\vec{\mu}_j \cdot \vec{R}_{ij})}{R_{ij}^5}\right] \tag{10}$$

Calculation of Absorption Spectra. To calculate the excitonic spectra of chlorophyll−dioxane and chlorophyll−water aggregates, two approaches were adopted. In the first the Q_y band positions and intensities were calculated by using the structural parameters of the aggregates from computed structures and the dipole−dipole interaction model. Excitonic energies were computed by diagonalizing 10×10 interaction matrixes **H′**. The diagonal elements H'_{ii} of **H′** are the $S_0 \rightarrow S_1$ transition energies of monomeric Chl *a* molecules (663 nm), and off-diagonal elements H'_{ij} of **H′** were calculated by using eq 10 and the structural parameters of the aggregates. The intensity of a transition is proportional to

$$\mu_K^2 = \sum_{i,j=1}^{N} |\vec{\mu}_i||\vec{\mu}_j|[\hat{\mu}_i \cdot \hat{\mu}_j] U_{iK} U_{jK} \tag{11}$$

Where $\vec{\mu}_i$ is the transition dipole moment vector in molecule *i*, $\hat{\mu}_i$ is a unit vector in the direction of that transition, $\vec{R}_{ij}$ is the position vector between the two dipoles, R_{ij} is the distance between two dipoles, and U_{iK} is *i*th element of the eigenvector for the *K*th exciton state.[23] In the second approach the minimum energy structures of dimers, trimers, and tetramers of each aggregate were taken from molecular mechanics calculation. Then using the semiempirical ZINDO/S method, the transition energies of these species with fixed geometry were calculated. All possible singly excited configurations from HOMO−14 to LUMO+14 were included. Calculated transition energies must be calibrated because, for example, 15 HOMO and 15 LUMO orbitals of a tetramer correspond to approximately four HOMO and four LUMO orbitals of each monomer, and 15 HOMO and 15 LUMO orbitals of a dimer correspond to approximately seven HOMO and seven LUMO orbitals of each monomer. Linear scaling of the calculated and experimental monomer transition energies was used to make comparisons of the transition energies between different molecular orbitals from the CI calculations and observed spectral values possible. Singlet excitation energies and oscillator strengths (*f*) were calculated by the ZINDO/S method. Excitation energies for the aggregates were computed by using 451 singly excited configurations. Theoretical spectra (estimated transition energy values) in Figures 12−14 are presented as bar charts showing transitions with *f* values greater than 0.01.

Results and Discussion

Spectroscopy of the Chl *a*−Dioxane Aggregate. Absorption spectrum of 5×10^{-5} mol/L Chl *a* in 3-methylpentane (3-MP) is indicative of a mixture of monomers and self-aggregates in solution (Figure la). The characteristic monomer Q_y band appears at 663 nm. Absorption from self-aggregated species is assigned to the slightly red-shifted shoulder located at 674 nm. By adding a small amount of dioxane in a dilute Chl *a* hydrocarbon solution, new aggregates are formed.[25] The absorption spectrum of the aggregates shows two separate bands at room temperature (Figure 1b), at 684 nm (a shoulder at 689.5 nm), and at 699 nm (the corresponding shifts are 463 and 777 cm^{-1} respectively). At liquid nitrogen temperature, both bands are split into doublets, one at 683 and 689 and the other at 698 and 702 nm (Figure 2). There seem to be only very small shifts of the absorption wavelengths from room temperature to liquid nitrogen temperature (77 K).[25] At low temperatures the

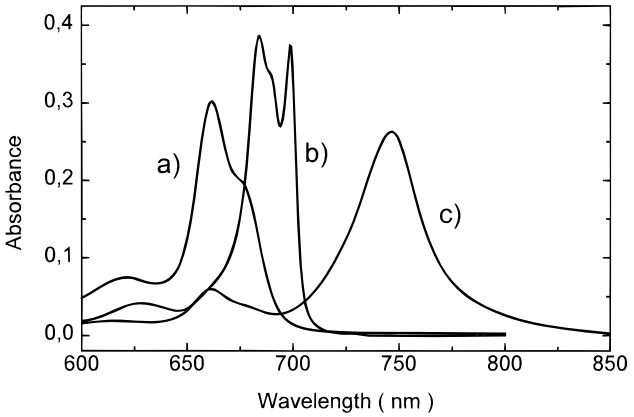

Figure 1. Absorption spectra of Chl *a* aggregates in 3-methylpentane at room temperature. (a) Chl *a* monomer and self-aggregate, 663 nm (monomer) and 674 nm (shoulder, self-aggregate). (b) Chl *a*−dioxane aggregate, 684 nm and 699 nm. (c) Chl *a*−water aggregate, 747 nm.

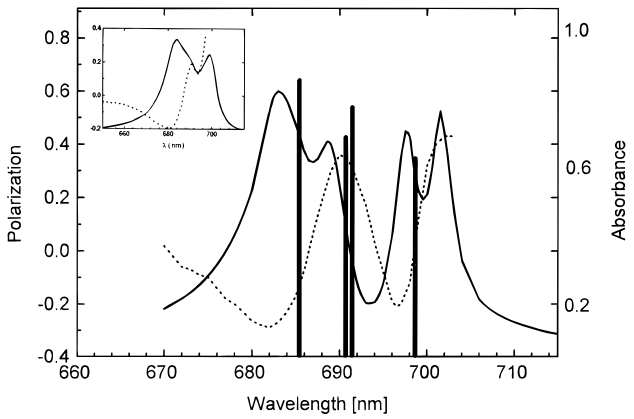

Figure 2. Experimental absorption (solid line), fluorescence excitation polarization (dotted line) spectra detected at 702 nm at 77 K and the computed absorption spectra of Chl *a*−dioxane aggregates. The computed stick spectrum of the two Chl *a*−dioxane tetramers is composed of two of the most intense transitions calculated by semiempirical ZINDO/S method. The stick pair on the left corresponds to the lsl-tetramer with calculated polarizations of −0.13 and +0.35, and the pair on the right to the sls-tetramer with calculated polarizations of −0.33 and +0.50. The structures of the two tetramers are shown in Figure 5. The inset shows the absorption spectrum (solid line) and fluorescence excitation polarization spectrum (dotted line) detected at 702 nm of the Chl *a*−dioxane aggregate at room temperature.

bandwidths of the components of the former doublet are about 95 cm^{-1} and for the latter about 50 cm^{-1}. The fluorescence excitation polarizations of the band pairs are 683(−0.29)/689 (+0.36) nm and 698(−0.21)/702(+0.43) nm are opposite in sign when observed at 702 nm.[25] The CD spectrum is strong and has one positive and two negative signals.[25] Excitation at 679 nm equally bleaches all four absorption bands.[26] The excitation fluorescence spectrum of the solution resembles closely the absorption spectrum. The observations suggest a single aggregate species to occur in solution. The dioxane aggregate has a fluorescence lifetime of 60 ps for the major emission band at 702 nm.

Computed Structure of the Chl *a*−Dioxane Aggregate. The monomer structures of Chl *a* and dioxane were optimized by using the semiempirical PM3 method. All structural parameters of Chl *a* were optimized including those of the phytyl tail. The main result was that in the minimum energy conformation in vacuum the phytyl tail is twisted above the porphyrin plane. This geometry of Chl *a* was then used as a starting geometry in the study of different aggregate structures under

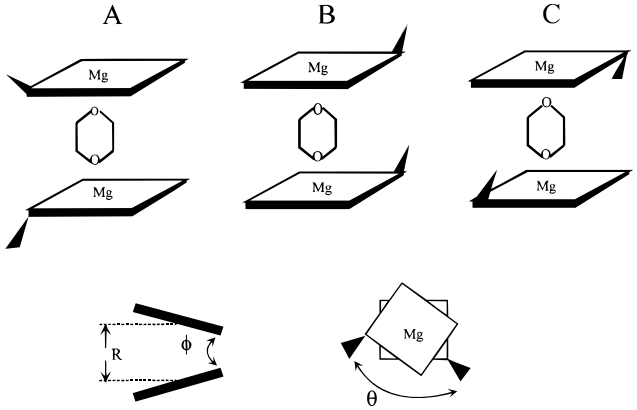

Figure 3. Schematic presentation of the computed Chl *a*−dioxane dimer structures with three possible orientations of the phytyl tails: (a) open dimer, (b) array dimer, (c) sandwich dimer. *R*, ϕ, θ (phytyl tail−phytyl tail angle) refer to structural parameters given in Table 1.

TABLE 1: Geometrical Parameters and Bonding Energies of Chl *a*−Dioxane Dimers

structure	Mg−Mg distance *R* [Å]	ϕ [deg]	θ [deg]	binding energy [kJ/mol]
A	6.5	0	90	78.3
B	6.7	50	90	59.9
C	7.5	0	180	112.8

molecular mechanics optimization. Dimers were studied first Figure 3 shows schematic presentations of three minimum energy structures of Chl *a*−dioxane dimers. In all dimers studied the dioxane molecule binds directly to the magnesium atoms of the adjacent chlorophylls. Table 1 lists Mg−Mg distances, dihedral and twist angles, and bonding energies of these dimers.

In the lowest energy dimer, which we call a sandwich dimer, the phytyl chains of the chlorophylls are oriented almost parallel in the space between the stacked porphyrin rings (Figure 3c). The distances between oxygen atoms of dioxane and Mg atoms of the chlorophylls are approximately 2.2 Å, and the distance between Mg−Mg atoms of the dimer is 7.52 Å. In the sandwich dimer the Q_y transition dipole vectors (taken to be 5.16 D, directed along N(A)−N(C) atoms of the porphyrin moiety) are almost parallel. The next stable dimer, which we call an open dimer, was the one with the two phytyl tails oriented in opposite directions (Figure 3a). In this dimer the porphyrin rings are not necessarily parallel, and this property finally determines the three-dimensional structure of larger aggregates. The distance between Mg−Mg atoms in the open dimer is 6.5 Å.

To build larger aggregates, the sandwich dimer was used as a building block. The open dimer appears in a tetramer, where a dioxane molecule binds two sandwich dimers together. In the tetramer the two sandwich dimers form an angle (angle θ in Figure 3) of 90° to each other. When the third sandwich dimer is stacked and energy mininized, the third sandwich dimer forms an angle of 90° with respect to the second dimer. For the fourth sandwich dimer the minimum energy structure gives an angle of 170° with respect to the third dimer. This sequence is periodically repeated in larger aggregates. Fine-tuning of the angles defining the porphyrin planes of the open dimer in the structure produced three minimum energy overall structures of aggregates including 24 monomer units (Figure 4). For example in the stick structure (Figure 4, top) porphyrin rings are approximately parallel, but in a ring structure (Figure 4, bottom) porphyrins are tilted about 20−25° (angle ϕ) with respect to each other. The distances between Mg−Mg atoms of the open dimer in the stick aggregate vary between 6.2 and 6.5 Å and between 6.2 and 6.7 Å in the ring aggregate. In both aggregates

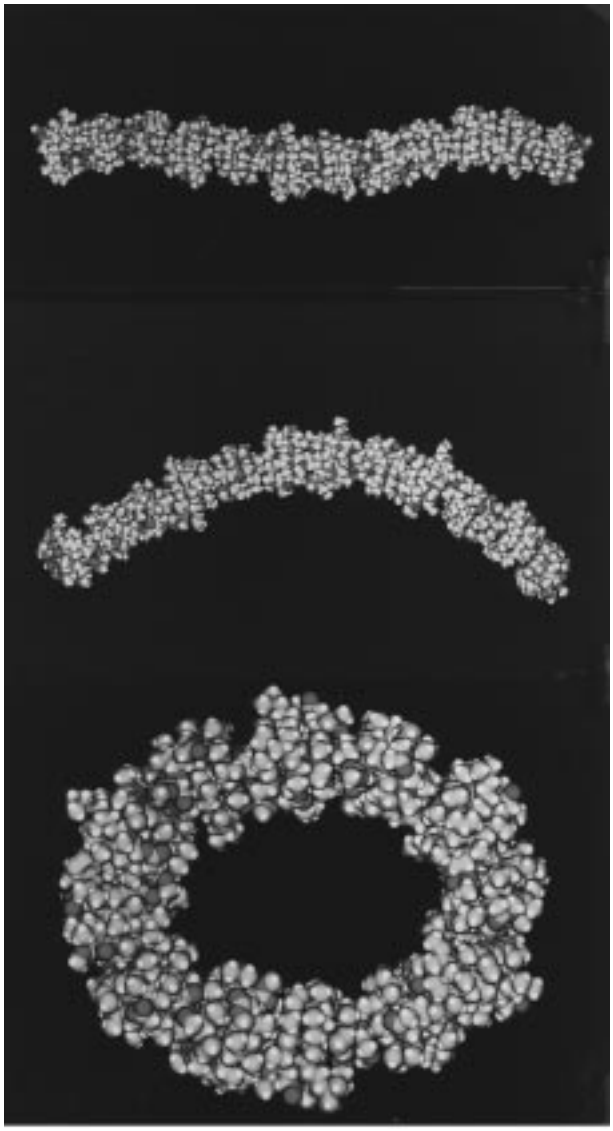

Figure 4. Computed minimum energy structures of (Chl *a*−dioxane)$_{24}$ aggregates. From top to bottom: stick. curved, and ring structure.

the Mg−Mg distances of the sandwich dimer vary between 7.3 and 7.9 Å. The average distance in all four computed aggregate structures for the open dimer is 6.4 Å (std. 0.2 Å) and for the sandwich dimer 7.6 Å (std. 0.2 Å). Statistically it is obvious then that two average distances and two dimers appear repeatedly in the structure. The transition moments of the monomers of the open dimer are roughly in opposite orientations, while they are roughly in parallel orientations in the sandwich dimer. In an earlier study significantly longer Mg−Mg distances of the Chl *a*−dioxane aggregate from 8 to 10 Å have been suggested.[24] If the phytyl tails of the sandwich dimer are forced out of the space between the porphyrin planes, the porphyrins of the dimer remain almost parallel, and the distance between Mg−Mg atoms (sandwich dimer) remains larger (from 7.0 to 7.4 Å) than that of the open dimer. Accordingly, the appearance of two different dimers in the structure is not a question of orientation of phytyl tails only but a question of orientation of the phytoxycarbonylethyl side chain relative to porphyrin plane.

As described above, all computed Chl *a*−dioxane aggregate structures contain two basic dimers with different geometry and orientation of the transition moments as internal heterogeneity. Two different tetramers are periodically repeated in the structure (Figure 5). In one tetramer (Figure 5a) there are two sandwich dimers and one open dimer (lsl-tetramer), while in the other (Figure 5b) there is one sandwich dimer and two open dimers (sls-tetramer). Observed internal heterogeneity is used next to calculate the absorption and polarization spectra of these Chl *a*−dioxane aggregate structures.

Exciton Interactions in Chlorophyll *a*−Dioxane Aggregates. The results of exciton theory with dipole−dipole interaction and with structural parameters from molecular mechanics calculations for three (Chl *a*−dioxane)$_{10}$ aggregates are given in Table 2. It is obvious that in each case a blue excitonic shift is predicted. The results indicate that the ring structure would produce the smallest blue shift. This is reasonable because magnesiun−magnesium distances are almost the same in all the structures, but in the ring structure the porphyrin planes form an angle (ϕ) of about 20° with respect to each other.

The detailed results for the stick aggregate (Table 3) show that the primary absorption bands of the Q_y transition of (Chl *a*−dioxane)$_n$ are at 663, 651, 647, 645, 651, 648, 647, 646, 645, and 648 nm for $n = 1, 2, 3, 4, 5, 6, 7, 8, 9,$ and 10, respectively. The calculated shifts do not agree with the experimentally observed absorption spectra of the Chl *a*−dioxane aggregate (Figure 1b), where two red-shifted peaks are found, one at 686 nm and one at 699 nm at room temperature. The primary reason for the calculated blue shift is that in the computed aggregate structure the porphyrin planes are almost on top of one another and form almost a zero angle (ϕ) with each other. For this reason the dot product $\vec{\mu}_i \cdot \vec{R}_{ij}$ (in eq 10) is approximately zero. Therefore the dipole−dipole interaction exciton calculation predicts a blue shift of the Q_y absorption band. Assuming that the stick aggregate in reality forms a three-dimensional log stack structure, where porphyrin planes of different stick aggregates are almost in line (the magnesium−magnesium distances of adjacent Chl *a* molecules not linked by dioxane are about 13 Å), then it seems possible that the model would produce red-shifted Q_y bands for Chl *a*−dioxane aggregates. These structures we have not so far being able to model reliably.

The calculated absorption spectra of the one-dimensional model structures of Chl *a*−dioxane aggregates obtained by using the semiempirical ZlNDO/S method are all red-shifted (Figures 6 and 7), in qualitative agreement with the experimental absorption spectrum (Figures lb and 2). The result is very different from what we obtained by using the exciton calculation for the same structure. The calculated Q_y band positions of Chl *a*−dioxane dimers are at 661 and 684 nm for the sandwich dimer (Figure 6, bottom spectrum), at 670 and 679 nm for the open dimer (Figure 6 middle spectrum), at 664, 674, and 689 nm for the trimer (Figure 7, top spectrum), at 685 and 691 nm for the 1sl-tetramer (Figure 7, middle spectrum, structure Figure 5a), and a strong doublet at 691 and 698 nm and two weaker bands at 706 and 716 nm for the sls-tetramer (Figure 7, bottom spectrum, structure Figure 5b). The shifts obtained for the two dimers and the trimer are smaller than the experimentally observed shifts.

The calculated shifts for the tetramers may be compared to the low-temperature absorption band pairs of the Chl *a*−dioxane aggregate at 683/689 and 698/702 nm, respectively. A single sls-tetramer substructure could be used to explain the quartet structure of the absorption spectrum of Chl *a*−dioxane aggregate. The computed spectrum of the sls-tetramer has four transitions with reasonable intensity (Figure 7, bottom). The computed shifts are slightly too large as compared to the experimental values. A blue shift of 190 cm^{-1} for all four computed transitions would bring the absorption bands at 682/

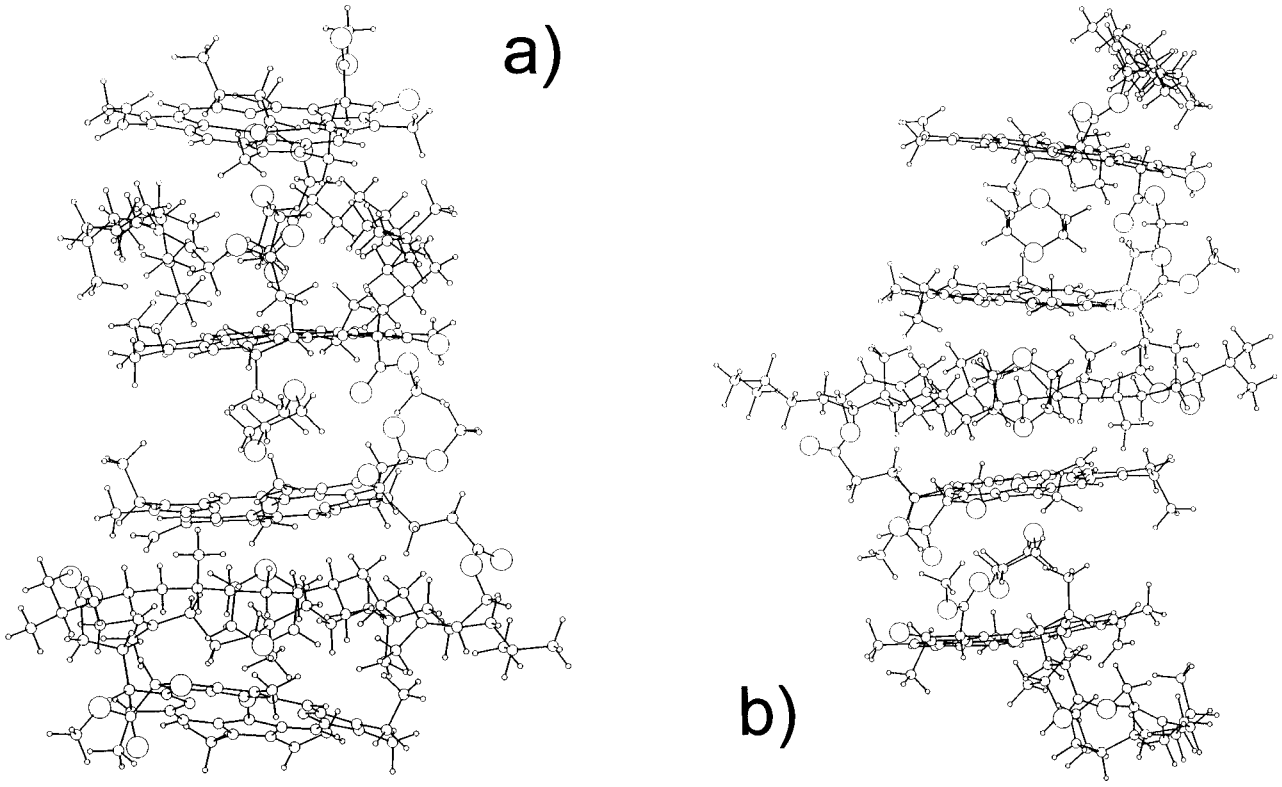

Figure 5. The two repeating tetramers of the Chl *a*−dioxane aggregate: (a) tetramer with two long and one short Mg−Mg distances (lsl-tetramer); (b) tetramer with one long and two short Mg−Mg distances (sls-tetramer). The orientations of the transition moments of the monomers in the two tetramers are approximately, starting from the bottom, (a) left, right, right, left and (b) right, left, right, left.

TABLE 2: Wavelengths and Relative Oscillator Strengths of the Q_y Bands of Three (Chl *a*−Dioxane)$_{10}$ Aggregates in Vacuum

(Chl *a*−dioxane)$_{10}$		(Chl *a*−dioxane$_{10}$		(Chl *a*−dioxane)$_{10}$	
stick (nm)	osc. str.[a]	curved (nm)	osc. str.[a]	ring (nm)	osc. str.[a]
642	(0.20)	643	(1.00)	647	(1.00)
645	(0.63)	646	(0.20)	648	(0.46)
648	(1.00)	652	(0.05)	656	(0.29)
652	(0.19)	655	(0.20)	659	(0.91)
660	(0.02)	658	(0.44)	660	(0.21)
669	(0.03)	672	(0.01)	668	(0.21)
676	(0.01)	673	(0.01)	671	(0.08)
680	(0.00)	677	(0.03)	673	(0.04)
683	(0.01)	678	(0.00)	678	(0.02)
687	(0.01)	683	(0.00)	679	(0.00)

[a] $F = (\mu_K^2)/(\mu_K^2)_{max}$.

689 nm and at 697/706 nm in good agreement with the experimental wavelengths. However, the transition at 697 nm in this case would have a wrong sign of polarization (+0.15) compared to the experimental value of −0.2.[25]

To acount for the experimental polarizations of the transitions, a model where both sls- and lsl-tetramers are included was developed. If we assume that the pigments of the aggregate are effectively coupled over four units at a given time, then statistical fluctuation would produce two different tetramers available for photon absorption. If the excitation is delocalized over four monomers, as has been suggested, for example, for the *Rb. sphaeroides* LH2 850 nm antenna,[27] then an absorption from each tetramer would be seen. Localization of excitation may be induced by the energy disorder of the aggregate. According to our calculations, more red-shifted absorption would arise from the sls-tetramer, while the less red-shifted absorption is from the lsl-tetramer of the aggregate. The calculated shifts for the lsl-tetramer (two most intense transitions, Figure 7, middle spectrum), are 484 and 611 cm^{-1}, and the corresponding experimental shifts are 442 and 569 cm^{-1}. The calculated shifts for the sls-tetramer are 569 and 756 cm^{-1} (two most intense transitions, Figure 7, bottom spectrum), and the corresponding experimental shifts are 756 and 838 cm^{-1}. The experimental and calculated shifts coincide reasonably well keeping in mind the limitations of the calculation. The experimental absorption and polarization spectra at 77 K including the computed spectrum are shown in Figure 2.

The structural models and the semiempirical calculation presented above may be used to predict the polarizations of the absorption bands. For the band pair 683/689 nm experimental polarizations are −0.29 and +0.36 and the computed polarizations of the lsl-tetramer are −0.13 and +0.35, and for the band pair 698/702 nm experimental polarizations are −0.21 and +0.43 and the computed polarizations of the sls-tetramer are −0.33 and +0.50. Both the signs and the magnitudes of the polarizations from the computed tetramer structures compare well with the experimental results.

The semiempirical calculations suggest that tetrameric disorder could in principle exist in the real structure of Chl *a*−dioxane aggregates in solution. It is interesting to note a similarity in the computed structure of the Chl *a*−dioxane aggregate and the LH2 850 nm antenna of *Rh. acidophila*. Both show Mg−Mg distance duality: in the aggregate we have two repeating distances of 6.4 and 7.6 Å, and in the antenna the two distances are 8.9 and 9.6 Å.[28] The perpendicular distances of the porphyrin planes are different in the two systems, about 6.5 Å in the aggregate and about 3.9 Å in the LH2 850 nm antenna.

Our Chl *a*−dioxane aggregate calculation shows quite clearly that the dipole−dipole interaction with the assumption that the Q_y transition dipole is taken to lie in the porphyrin plane[9] may

TABLE 3: Wavelengths and Relative Oscillator Strengths of the Q_y Bands of (Chl *a*−Dioxane) Aggregates (n = 2, ..., 10) in Vacuum

	λ [nm] F^a									
dimer	651	677								
	1	0.06								
trimer	647	664	681							
	1	0.46	0.02							
tetramer	645	655	673	683						
	1	0.88	0.00	0.00						
pentamer	644	651	664	677	685					
	0.69	1	0.10	0.03	0.03					
hexamer	643	648	658	671	680	686				
	0.48	1	0.19	0.03	0.00	0.00				
heptamer	642	647	654	664	674	681	687			
	0.38	1	0.39	0.01	0.05	0.01	0.01			
octamer	642	646	651	659	669	677	682	687		
	0.27	1	0.64	0.01	0.05	0.00	0.00	0.01		
nonamer	642	645	650	657	664	671	679	683	687	
	0.27	1	0.88	0.07	0.11	0.02	0.02	0.01	0.01	
decamer	642	645	648	652	660	669	676	680	683	687
	0.20	0.63	1	0.19	0.02	0.03	0.01	0.00	0.01	0.01

[a] $F = (\mu_K^2)/(\mu_K^2)_{max}$.

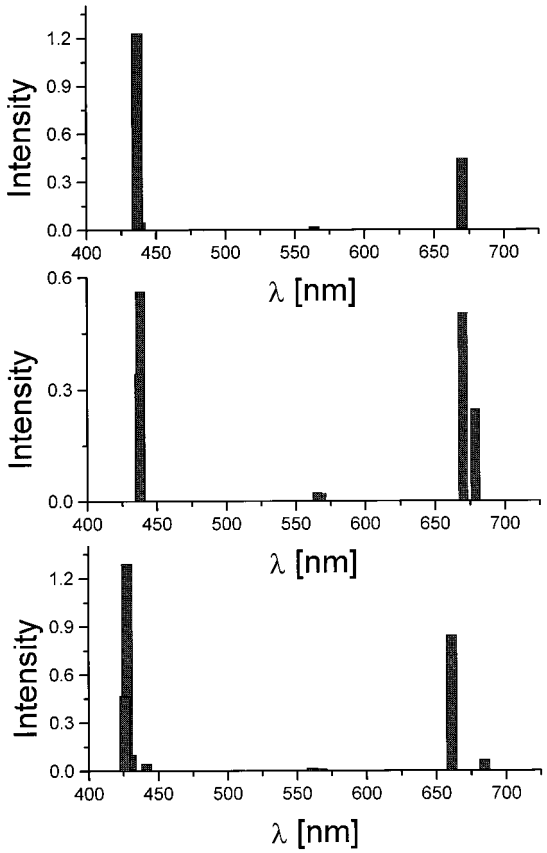

Figure 6. Computed absorption spectra of Chl *a*−dioxane aggregates from top to bottom: monomer, open dimer, sandwich dimer.

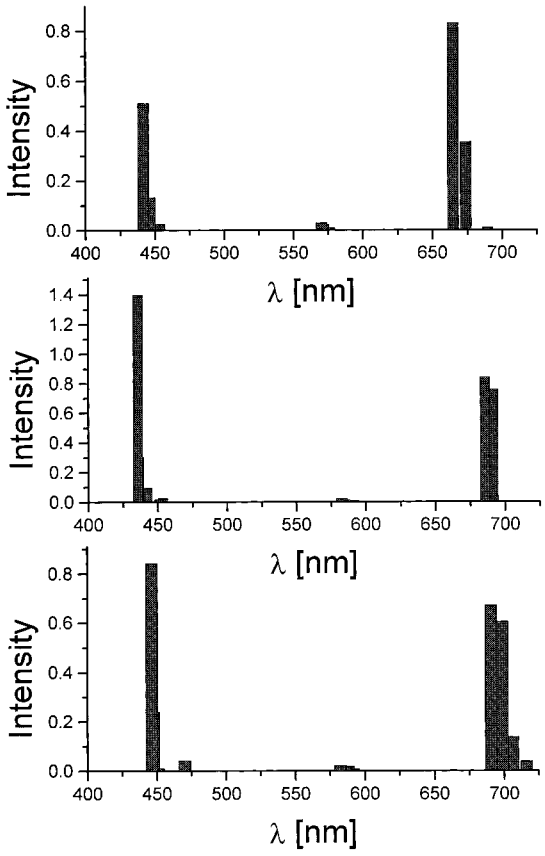

Figure 7. Computed absorption spectra of Chl *a*−dioxane aggregates from top to bottom: trimer, lsl-tetramer, sls-tetramer.

not correctly describe the interaction between the electronic states of the closely packed Chl's. For our model structures the exciton calculation predicts only blue-shifted transitions (Table 3). The semiempirical CI method gives for the same geometry only red-shifted Q_y transitions (Figures 6 and 7). One of the differences between the two methods is that the semiempirical CI method gives a transition moment for the monomer Chl *a* in vacuum that *does not* lie in the porphyrin plane. The effect of the linker molecule on the electronic states of the Chl's is also taken into account in the semiempirical calculation. The Q_y transition energy of the (Chl *a*−dioxane$_2$) complex is red-shifted by 111 cm^{-1} and has a larger excited-state dipole moment by 0.5 D as compared to the excited-state dipole moment of Chl *a* monomer. Other properties such as the direction and magnitude of the transition dipole, however, remain almost the same in a single Chl *a* and the (Chl *a*−dioxane$_2$) complex. In the aggregates (Chl *a*−dioxane)$_n$ with $n \geq 2$ the semiempirical CI method treats the aggregate as a supermolecule and defines their spectroscopic properties according to the wave functions of the supermolecule. These wave functions contain the effects from the linker molecules in the transitions involved. This approach is clearly to be used in cases where chromophores

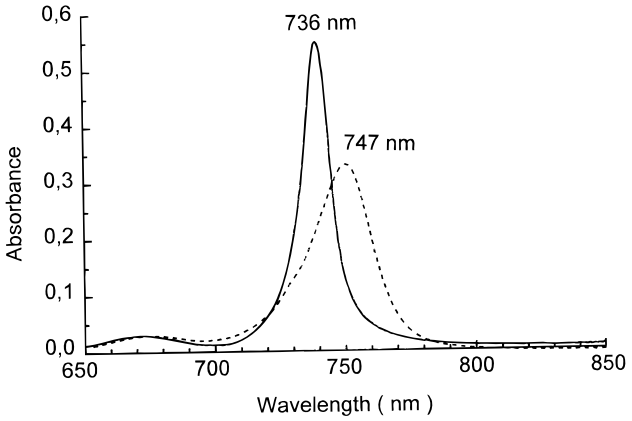

Figure 8. Room (dashed line) and liquid nitrogen temperature (solid line) absorption spectra of Chl *a*−water aggregate in 3-methylpentane.

are in close contact with each other. It seems that in estimating exciton interactions in in vivo light harvesting systems interactions between the surrounding molecules and the chromophore have to be taken into account. Our results suggest that the orbital overlap between the chromophores (chlorophylls, bacteriochlorophylls, and carotenoids) and the protein in a photosynthetic light harvesting antenna may play an important role in determining spectral and energy-transfer properties of these complexes.

Spectroscopy of Chl *a*−Water Aggregate. Addition of water into a 5×10^{-5} mol/L solution of Chl *a* (Chl *a*/water molar ratios from 1:20 to l:60) in 3-methylpentane results in a strongly red-shifted band at 747 nm (Figure 1c). The total red shift with respect to the monomer band is 84 nm (1680 cm^{-1}). At the same time the Soret absorption band of the monomer at 430 nm is shifted to 450 nm, corresponding to a total shift of 1034 cm^{-1}. The shifted bands arise from Chl *a* water aggregates in solution.[29,30] The full-width at half-maximum (fwhm) of the aggregate Q_y absorption varies from 500 to 600 cm^{-1} at room temperature, depending on the preparation. At liquid nitrogen temperature (77 K) the Chl *a*−water aggregate absorption band is blue shifted by 200 cm^{-1} to 736 nm from the room-temperature spectrum. The half-width of the absorption band is strongly reduced to about 240 cm^{-1} (Figure 8). We suggest that lowering the temperature reduces the solvent interaction between the aggregate and the excess water in the aggregate and gives rise to the blue shift. The narrowing of the line width is indicative of strong coupling of phonons or low-frequency vibrational modes to the electronic states involved.

The fluorescence spectrum of the Chl *a* water aggregate peaks at 753 nm. The quantum yield is about 1000 times lower than the quantum yield of the monomer chlorophyll *a* in solution.[31] A laser-excited fluorescence experiment on the Chl *a*−water adduct in 3-MP shows that the wavelength of the fluorescence maximum is independent of the excitation wavelength. Any excitation between 710 and 745 nm produces the same fluorescence band with the emission maximum at 753 ± 0.5 nm (room temperature), Figure 9. It was not possible to measure the fluorescence of the extreme red edge of the absorption band because of the low OD used in the fluorescence experiment and the low quantum yield of the aggregate. The excitation-independent emission wavelength suggests that the excitation energy relaxes to a low lying state from where weak emission takes place.

A possible mechanism to explain the excitation-independent emission spectrum could be energy transfer among closely packed individual aggregates with some energetic disorder.

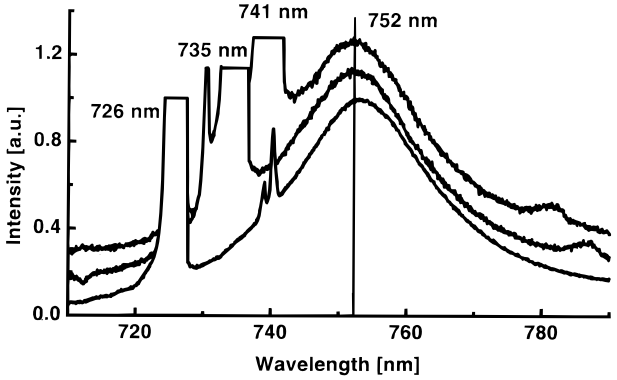

Figure 9. Site-selective fluorescence spectra of Chl *a*−water adduct in 3-methylpentane at 298 K. Fluorescence maximum is at 753 ± 1 nm independent of the excitation wavelength between 710 and 745 nm. Fluorescence maximum is normalized to a value of 1.0, and the laser lines in the figure have been cut off at the same value. The sharp feature after the 726 nm laser excitation band originates from a defect in the CCD used.

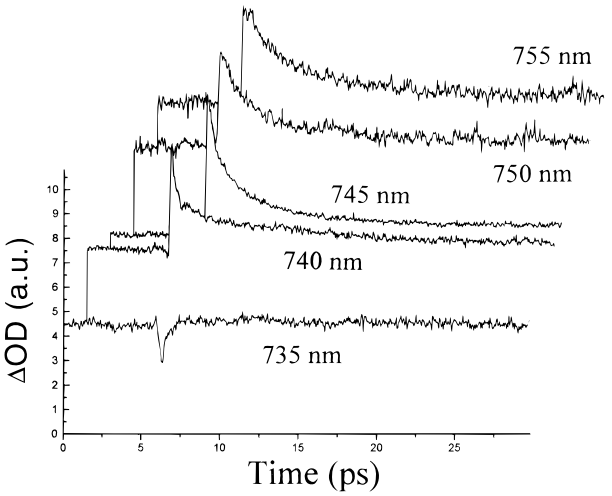

Figure 10. Wavelength dependent femtosecond relaxation of Chl *a*−water aggregates at RT. The negative signal at 735 nm is due to the excited-state absorption.

According to this model, the excitation energy would be transferred to the most red-shifted aggregate in a manner similar to that observed in the photosynthetic light harvesting antenna. Another explanation for the observed excitation-independent emission spectrum is that the blue edge of the absorption band arises from the higher exciton states predicted by semiempirical calculation of the Chl *a*−water adduct. In this case the relaxation would be among the exciton states of a single aggregate and the emission would come from the lowest exciton state.

The single-color absorption recovery signal of the Chl *a*−water aggregate is wavelength dependent, showing an evident sub-picosecond component on the blue side of the Q_y band (740 nm) that disappears as one moves to the red side of the absorption band (760 nm). At 735 nm we see absorption from the excited state (Figure 10). The shortest resolved (three-exponential fit) lifetime components at wavelengths 760, 755, 750, and 740 nm were 2.0(67%), 1.0(31%), 0.6(12%), and 0.2-(14%) ps; the next longest components were 12(12%), 4.2(37%), 3.5(69%), and 1.8(40%) ps, respectively. All signals contained a third component with a lifetime longer that 25 ps, which was not well determined within the delay region of 30 ps used in these measurements and is due to an unidentified long-lived state (probably a triplet state). The wavelength dependence of

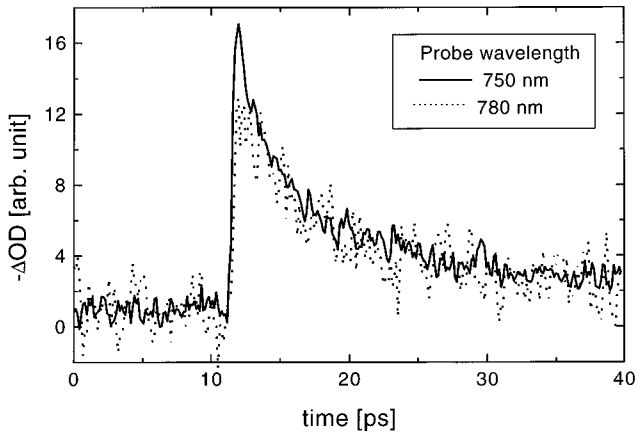

Figure 11. Two-color pump and probe signals from the Chl *a*−water aggregates at RT. Excitation from a titanium-sapphire femtosecond laser at 725 nm. Probe wavelengths were 750 and 780 nm. Pulse duration of 350 fs was estimated from the rise time of the signal. The rise time remained constant at various wavelengths.

the femtosecond relaxation of the absorption band may have contributions from (a) decay from the higher excitonic states to the final emitting state, (b) energy transfer between closely packed aggregates with energetic disorder, and (c) ultrafast spectral shift taking place as the solvation in the aggregate relaxes to the final equilibrium after excitation. To differentiate between these mechanisms, two-color experiments, preferably with sub-100 fs excitation, are needed. In this manner the growth of solvent relaxation and/or stimulated emission in the red side of the absorption band could possibly be resolved. Solvent contribution could be reduced by carrying out the experiments at low temperatures.

Two-color pump−probe experiments where the blue side of the Q_y band of the Chl *a*−water adduct was excited at 725 nm and probed at 10 nm intervals between 740 and 780 nm (Figure 11) were performed at room temperature. The bleaching signal was best fitted with a 350 fs Gaussian pulse as an instrumental function at each wavelength. With this time resolution the bleaching of the main red absorption band of the Chl *a*−water adduct appears to be simultaneous over the whole wavelength range from 740 to 780 nm. No change in the rise time of the signal was observed when moving from 740 to 780 nm. The fastest decay component changes gradually from 2.2 ps (740 nm), 2.3 ps (750 nm), 2.3 ps (760 nm), 2.7 ps (770 nm) to 3.0 ps at 780 nm. A two-exponential fit produces an additional decay component of 10−15 ps. We expect that there is an ultrafast spectral shift due to solvent relaxation and equilibration of excitation energy that we fail to observe in the two-color experiment because of limited time resolution and signal-to-noise ratio. Anyhow, it is clear from this data that when excited at 725 nm, the absorption spectrum is bleached within 350 fs.

Laser-induced fluorescence spectra together with the two-color pump−probe experiment are in agreement with the idea that the Q_y absorption band of the Chl *a*−water adduct consists of a strong transition with lowest energy and several weaker higher energy transitions on the blue side of the absorption band. This interpretation is also in agreement with the previously measured time-dependent anisotropy and linear dichroism data. A single-color pump−probe experiment at 743 nm produced a rather high 0.25 residual anisotropy of the bleaching signal.[31] This indicates that after the equilibration spatial correlation remains between the originally excited transition and the equilibrated state. In the static linear dichroism (LD) spectrum of the Chl *a*−water adduct oriented in a flow of paraffin oil the reduced LD $[(A_{||} - A_{\perp})/(3A_{iso})]$, where the A_{iso} is the absorbance of the randomly polarized light, is clearly stronger on the red side than on the blue side of the absorption band.[28,30] With the data available we cannot rule out a possibility of energy transfer between closely packed aggregates as an explanation for the wavelength dependence of the time-resolved experiments. This being the case, the packed aggregates have to be highly ordered to account for the observed high residual anisotropy of the bleaching signal.

Computed Structure of the Chl *a*−Water Aggregate. Computing the structure of the Chl *a*−water aggregate is much more difficult than that of the Chl *a*−dioxane aggregate because Chl *a* and water molecules can form many different initial structures, as has been reported previously.[33,34] We started the simulation by using a model where one water molecule binds two chlorophyll *a* molecules together. The starting dimer geometry was taken from the crystal structure of chlorophyllidine *a*.[8] At early stages the (Chl *a*−water)$_n$ aggregate evolved with a one-dimensional belt-like structure (Figure 12), where the water molecule binds to the central Mg atom and to the keto oxygen of the neighboring Chl *a* (oxo group at position C-13^1). The Mg−O (water) distance is about 2.19 Å, and the O (keto)−H (water) is about 2.17 Å. The magnesium−

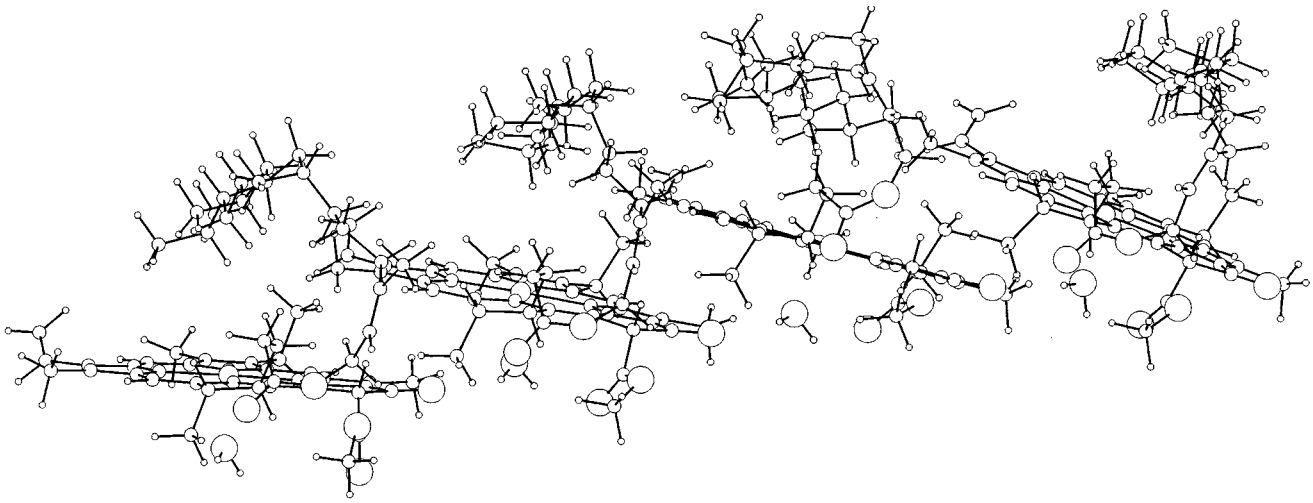

Figure 12. Computed structure of the Chl *a*−water tetramer, (Chl *a*−H_2O)$_4$. Oxygen atoms of the chlorophylls are organized along the bottom edge form a hydrophilic part and the phytyl tails along the top edge form a hydrophobic part of the aggregate.

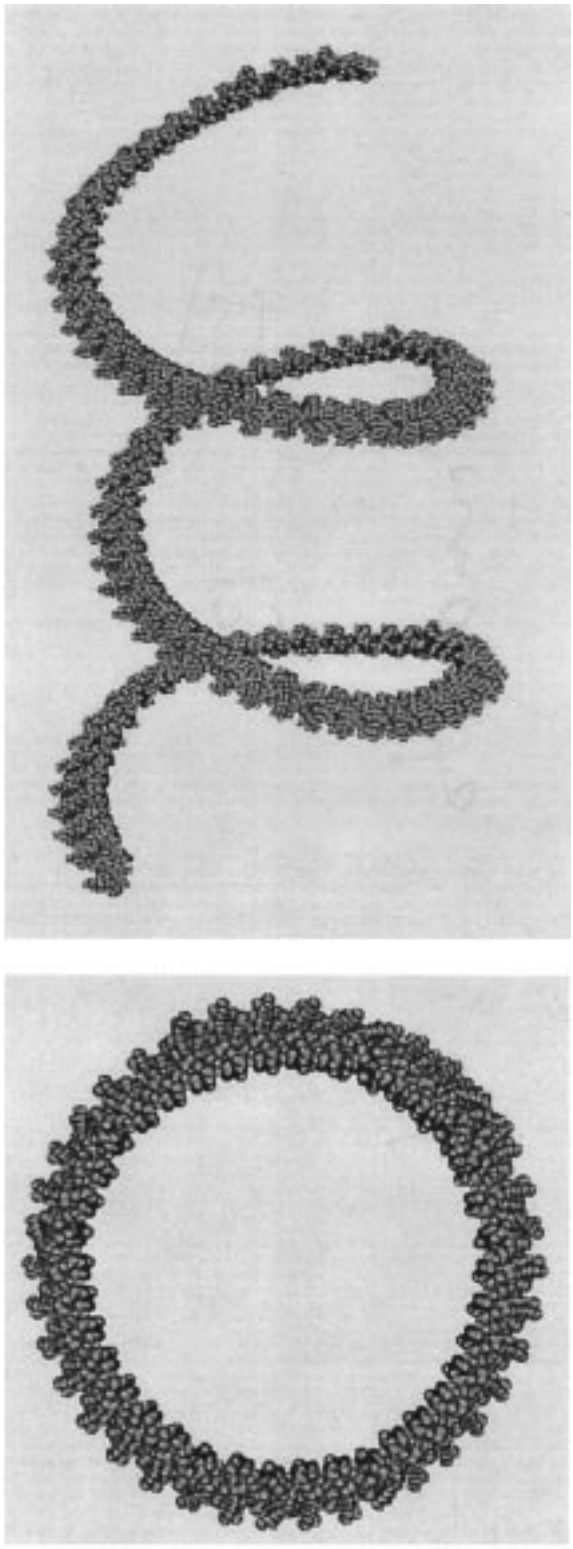

Figure 13. Computed helical structure of the Chl *a*−water aggregate, (Chl *a*−H_2O)$_{96}$. The helix radius is about 6 nm. One full turn rise is about 12 nm, and it contains 38 chlorophyll *a* molecules

magnesium distances in the aggregate vary from 9.2 to 9.4 Å. The perpendicular distance between the porphyrin planes is about 3.3 Å. The oxygen atoms of the porphyrins are nicely oriented on one side of the aggregate, forming a hydrophilic site for polar molecules to bind (Figure 12). As the aggregate size increases, the one-dimensional structure turns into a helix with a diameter of 12.0 nm, an increase of 12.4 nm per full turn (Figure 13) with 38 Chl *a* monomers. The helix diameter is very close to the diameter of 11.4 nm of tube-like structures of Chl *a*−water aggregates in hydrocarbon solution determined experimentally by neutron diffraction.[35] In the helix structure, the Q_y transition dipole vectors form an angle of about 5° with each other. It is quite possible that a helical one-dimensional aggregate serves as a building block for a tube-like structure assumed to occur in solution.[35] We estimate that 12 adjacent helixes are needed to form a closed tubular structure of a Chl *a*−water aggregate with roughly 3500 chromophores per 100 nm of such tube. In such a tube oxygen atoms of the chlorophylls would be pointing toward the inside of the tube (Figure 13, bottom). A hollow polar environment would serve as an excellent trap for the excess water molecules to escape from hydrocarbon solution. Water density gives a volume of a water molecule of about 30 Å^3. To fill a cylindrical cavity of radius 6 nm and length 100 nm, some 380 000 water molecules are needed. This means that in the aggregate there would be some 100 water molecules per one chlorophyll molecule. Experimentally we have found that water aggregates begin to form with Chl *a*−water ratios of 1:20−60 in 3-methylpentane solution, in good agreement with the tube-filling model. The estimate for the tube length from the neutron diffraction studies is 200 nm or longer.[35]

Exciton Interactions in the Chlorophyll *a*−Water Aggregate. The characteristic monomer Q_y absorption band of Chl *a* appears at 663 nm in a hydrocarbon solution. A small amount of water in the solution creates a Chl *a*−water adduct that shows a strongly red-shifted Q_y absorption band at 747 nm (Figure 1c).[29,30] The total red shift of the Q_y absorption band is 1680 cm^{-1}. At the same time the Soret absorption at 430 nm of the monomer pigment is red-shifted to 450 nm, about 1030 cm^{-1} in the aggregate.

For the (Chl *a*−H_2O)$_n$ structure our exciton calculations (Table 4) give the primary absorption bands of the Q_y transitions at 675, 682, 685, 687, 688, 689, 690, 691, and 692 nm for n = 2, 3, 4, 5, 6, 7, 8, 9, and 10, respectively. The corresponding values of Chow et al.[8] are 674, 679, 682, 684, 686, 687, and 687 nm for n = 2, 3, 4, 5, 6, 7, and 8, respectively, and those of Shipman et al.[9] 693, 703, 709, 712, 714, 715, 716, 717, and 718 nm for n = 2, 3, 4, 5, 6, 7, 8, 9, and 10, respectively. Our values are a little more red-shifted than those of Chow et al. The primary reason for the difference is the use of different structural parameters in each case. Chow et al. used coordinates of polymers found in the crystalline chlorophyllidine *a* dihydrate;[8] ours are based on the results from molecular mechanics calculation with one binding water molecule per monomer pair. In the Shipman et al. calculations an environmental shift was included; they used H_{ii} = 14 580 cm^{-1} (686 nm) for $i \geq 2$. Including an environmental shift of 200 cm^{-1} in the exciton calculation (eq 8) for the one-dimensional (Chl *a*−water)$_{10}$ aggregate gives a shift of 797 cm^{-1} of the Q_y band (Table 5). This is only one-half of the experimentally measured shift of 1680 cm^{-1}.

The calculated spectra of the small Chl *a*−water aggregates using the ZINDO/S method are shown in Figure 14. The calculated intensity of the main Q_y band is strong, very similar to what is observed in the experimental spectrum. The dimer (Figure 14, second spectrum from top), trimer (Figure 14, second spectrum from bottom), and tetramer (Figure 14, bottom spectrum) bands are red-shifted by 334, 632, and 756 cm^{-1}, respectively, as compared to the monomer band at 663 nm. The tetramer shift is roughly one-half of the experimental shift for the Chl *a*−water aggregate, but it is clearly larger than that predicted from the exciton theory (Tables 4 and 5). The

TABLE 4: Wavelengths and Relative Oscillator Strengths of Q_y Bands of (Chl *a*−Water)$_n$ Aggregates (n = 2, ..., 10) in Vacuum

	λ [nm] F^a									
dimer	653	675								
	0.02	1								
trimer	648	662	682							
	0.03	0.02	1							
tetramer	646	656	669	685						
	0.00	0.05	0.03	1						
pentamer	645	653	662	674	687					
	0.00	0.01	0.06	0.05	1					
hexamer	645	650	657	667	678	688				
	0.00	0.01	0.01	0.05	0.08	1				
heptamer	645	648	654	662	671	681	689			
	0.00	0.00	0.02	0.01	0.04	0.10	1			
octamer	644	647	652	658	666	674	683	690		
	0.00	0.00	0.01	0.02	0.02	0.04	0.13	1		
nonamer	644	646	650	655	662	669	677	685	691	
	0.00	0.00	0.00	0.01	0.01	0.03	0.04	0.17	1	
decamer	644	646	649	654	659	665	671	619	686	692
	0.00	0.00	0.00	0.00	0.01	0.01	0.04	0.03	0.22	1

[a] $F = (\mu_K^2)/(\mu_K^2)_{max}$.

TABLE 5: Wavelengths and Relative Oscillator Strengths of Q_y Bands of (Chl *a*−Water)$_n$ Aggregates (n = 2, ..., 10) with an Environmental Shift ($\sim$200 cm^{-1})

	λ [nm] F^a									
dimer	656	680								
	0.05	1								
trimer	653	666	688							
	0.06	0.03	1							
tetramer	652	660	675	693						
	0.01	0.07	0.04	1						
pentamer	652	658	667	680	695					
	0.01	0.02	0.07	0.05	1					
hexamer	652	656	662	673	685	697				
	0.01	0.02	0.02	0.06	0.07	1				
heptamer	651	654	660	668	677	689	698			
	0.01	0.01	0.03	0.02	0.05	0.09	1			
octamer	651	653	658	664	672	681	691	699		
	0.00	0.01	0.01	0.02	0.02	0.05	0.12	1		
nonamer	651	653	657	661	668	676	684	693	700	
	0.00	0.01	0.01	0.02	0.01	0.03	0.04	0.16	1	
decamer	651	652	656	660	665	672	678	687	694	700
	0.00	0.00	0.01	0.01	0.02	0.01	0.04	0.03	0.21	1

[a] $F = (\mu_K^2)/(\mu_K^2)_{max}$.

quantum chemical calculation includes in part the environmental shift that comes from the overlap of the neighboring chlorophyll orbitals and the bonding water molecule. According to the semiempirical calculation, the environment-induced red shifts are for both the Q_y and the Soret absorption bands of the aggregates, which is also observed experimentally.

The red shift of the absorption band of the Chl *a*−water aggregate can only partly be explained by the one-dimensional structural model we have used both in the framework of the exciton theory and in the semiempirical calculations. The rest of the red shift has to be explained by interactions of the neighboring chlorophyll pigments in the three-dimensional structure of the real aggregate. The tubular structure suggested above and the exciton model may be used as a starting point in estimating contributions from these interactions. Excess water assumed to be inside the hollow aggregate may also give rise to its own shift that was not estimated here.

Comparison of Spectroscopy of the Chl *a*−Water Aggregate and Chlorosomes of Green Bacteria. The in vitro Chl *a*−water adduct has received a lot of interest because its spectroscopic properties resemble closely those of the chlorosome antenna of green photosynthetic bacteria. The chlorosomes are flattened ellipsoidal bodies with dimensions about (100−260) × (30−70) × 12 nm.[36] These antennae contain bundles of highly aggregated Bchl (Bchl *c*, *d*, or *e* depending on the species) molecules organized in rod-like elements. In addition to the Bchl *c* pigments the chlorosomes contain protein, lipids, carotenoids, and BChl *a*. Chlorosomes can be imitated by in vitro BChl *c* aggregates, which has lead to an idea that the spectral properties of chlorosomes are determined solely by aggregated Bchl *c* (except for the BChl *a* and carotenoid absorption).[37,38] The role of protein in these bacterial antennae is still under discussion. The fact that these natural light harvesting systems can be imitated by in vitro aggregates of Bchl and that very similar aggregates can be built from Chl *a* has raised interest in the structure and spectroscopic properties of the artificial aggregates.

The similarities in optical behavior of in vitro Bchl *c*− and Chl *a*−water adducts extend from strongly red-shifted absorption spectra, similar CD spectra and linear dichroism spectra,[13] and fast excited-state kinetics to nearly identical physical dimensions. According to small-angle neutron scattering results, both aggregates are cylindrical objects with a diameter of 11.4 nm (Chl *a*) and 11.8 nm (Bchl *c*), respectively.[35]

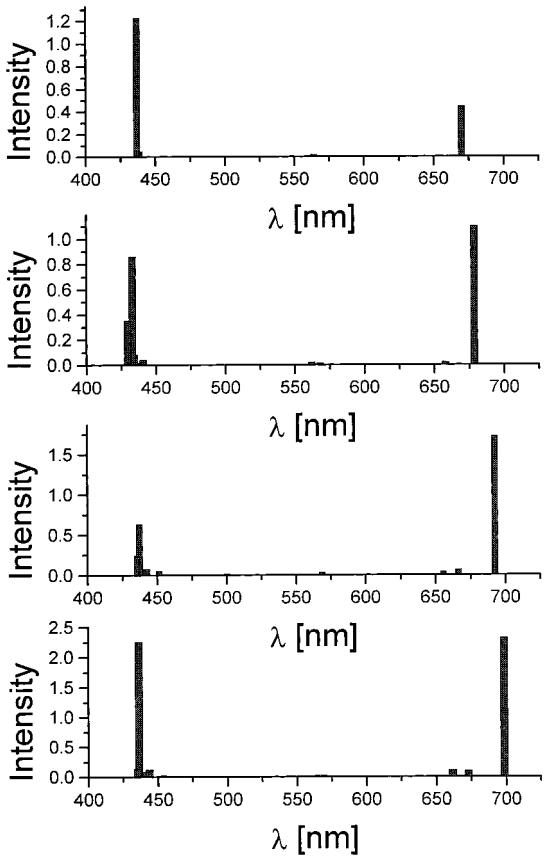

Figure 14. Computed absorption spectra of Chl *a*−water aggregates from top to bottom: monomer, dimer, trimer, and tetramer.

The fwhm of the Chl *a*−water adduct absorption band is about 500−600 cm^{-1} (at room temperature). It is of the same order of magnitude as the width of the long-wavelength band of the chlorosome absorption (e g., *Chloroflexus aurantiacus* about 700 cm^{-1}).[39] In the case of the absorption spectrum of the chlorosomes the hole-burning results show that narrow holes can only be burned in the red edge of the absorption band.[40,41] The width of the distribution of these narrow holes is about 90−100 cm^{-1}. The narrow hole is accompanied by a broad hole that follows the envelope of the absorption band. This observation is explained by taking the 100 cm^{-1} width as an inhomogenous distribution of lowest energy exciton component. The blue part of the absorption band then corresponds to higher exciton states. Both the time-resolved (excited-state lifetimes) and static spectroscopy (absorption and linear and circular dichroism) of the Chl *a*−water adduct suggest that the electronic structure is very similar to that of chlorosomes. The main difference is that the electron−phonon coupling in the Chl *a*−water adduct seems to be much stronger because the fwhm of the absorption band gets narrower by a factor of 2 when the temperature is lowered to 77 K. In the case of chlorosome antennae the width of the absorption remains almost constant down to 4 K.[40]

Conclusions

We have studied aggregates of Chl *a* with dioxane and water as interchromophore linker molecules. The results from absorption spectroscopy and from the quantum mechanical calculations are suggestive of tetrameric substructure present in the dioxane aggregates. The exciton theory with dipole−dipole interaction approximation gives blue-shifted transitions for the computed aggregate up to 10 monomeric units. For small aggregates from dimers to tetramers the semiempirical CI calculation gives only red-shifted transitions with strong oscillator strengths. Two computed tetrameric structures were used as models to explain the experimentally observed spectral shifts and polarizations of the dioxane aggregate absorptions observed at 77 K. It is possible that such terameric substructure is present in the real aggregate. For the Chl *a*−water aggregate the observed spectral shift is much larger, 1680 cm^{-1}, and the calculated shift of the one-dimensional model structure is only one-half of the observed shift. This we ascribe to the inadequacy of our one-dinensional model to describe the real Chl *a*−water aggregate. For water aggregates, polarized spectroscopy and neutron diffraction suggest a long tube-like structure of the aggregates. Our one-dimensional Chl *a*−water aggregate model shows a helical structure with a circular diameter of 12 nm, close to the experimental observed diameter of 11.4 nm of the real aggregates in solution. Twelve helixes would be needed to create a hollow tube with a very polar interior that would be able to draw excess water from hydrocarbon solution that is needed to from these aggregates. Internal water is suggested to induce a solvent shift in the aggregate spectrum at low temperatures.

The excitation-independent emission spectrum of the Chl *a* adduct suggests that the excitation energy is transferred to a low-energy state from where the emission occurs. The linear dichroism spectrum of the Chl *a*−water adduct[25] combined with the femtosecond pump−probe results[31] has lead us to suggest that the blue wing of the Chl *a*−water adduct absorption consists of higher exciton states of the aggregate. Femtosecond relaxation in the blue edge of the Chl *a*−water aggregate spectrum may be a combined effect of thermalization between the excitonic states and ultrafast spectral shift after excitation as the solvent relaxation in the excited state. With the results available we cannot exclude the possibility of energy transfer between the closely packed aggregates as a source of wavelength dependent ultrafast relaxation.

Acknowledgment. The Science (Contract No. SCI-CT92-0796) and HCM (Contract No. ERBCHB6CT930361, J.-L.G.) grants from the European Union 3rd and 4th research programs and financial support from the Academy of Finland (J.L.) are gratefully acknowledged. T.P. acknowledges the Nordic Energy Program for Artificial Photosynthesis for a scholarship. The authors acknowledge Prof. Rienk van Grondelle for providing the facilities for measuring the site-selective fluorescence spectra and the two-color femtosecond absorption recovery data.

References and Notes

(1) Ballschmiter, K.; Truesdell, K.; Katz, J. J. *Biochim. Biophys. Acta* **1969**, *184*, 604.

(2) Katz, J. J.; Shipman, L. L.; Cotton, T. M.; Janson, T. R. In *The Porphyrins: Physical Chemistry;* Dolphin, D., Ed., Academic Press: New York, 1978, Part C, Vol V, p 401.

(3) Cotton, T. M.; Loach, P. A.; Katz, J. J.; Ballschmiter, K. *Photochem. Photobiol.* **1978**, *27*, 735.

(4) Helenius, V. M.; Hynninen, P. H.; Korppi-Tommola, J. E. I. *Photochem. Photobiol.* **1993**, *58*, 867.

(5) Holzwarth, A. R.; Schaffner, K. *Photosynth. Res.* **1994**, *41*, 225.

(6) Kasha, M. Rawls, H. R.; Ashraf El-Bayoumi, M. *Pure. Appl. Chem.* **1965**, *11*, 371.

(7) Davidov, A. S. *Theory of Molecular Excitations;* McGraw Hill: New York, 1962.

(8) Chow, H.-C.; Serlin, R.; Strouse, C. E. *J. Am. Chem. Soc.* **1975**, *97*, 7230.

(9) Shipman, L. L.; Katz, J. J. *J. Phys. Chem.* **1977**, *81*, 577.

(10) Shipman, L. L.; Cotton, T. M.; Norris, J. R.; Katz, J. J. *J. Am. Chem. Soc.* **1976**, *98*, 8222.

(11) McDermott, G., Prince, S. M.; Feer, A. A.; Hawthornthwaite-Lawless, A. M.; Papiz, M. Z.; Cogdell, R. J.; Isaacs, N. W. *Nature* **1995**, *374*, 517.

(12) Koepke, J.; Hu, X.; Muenke, C.; Schulten, K.; Michel, H. *Structure* **1996**, *4*, 581.

(13) Oksanen, J. A. I.; Helenius, V. M.; Hynninen, P. H.; van Arnerongen, H.; Korppi-Tommola, J. E. I.; van Grondelle, R *Photochem. Photobiol.* **1996**, *64*, 356.

(14) Stewart, J. J. P. *J. Comput. Chem.* **1989**, *10*, 209.

(15) SPARTAN, Version 3.1, Revision A; Wavefunction Inc.; Irvine, CA, 1993, 1994.

(16) Stewart, J. J. P. *QCPE Bull.* **1985**, *5*, 133.

(17) Brooks, B. R.; Bruccoleri, R. E.; Olafson, B. D.; States, D. J.; Swaminathan S.; Karplus, M. *J. Comput. Chem.* **1983**, *4*, 187.

(18) Ridley, J. E.; Zerner, M. C. *Theor. Chim. Acta (Berlin)* **1973**, *32*, 111.

(19) Ridley, J. E.; Zerner, M. C. *Theor. Chim. Acta (Berlin)* **1976**, *42*, 223.

(20) Zerner, M. C.; Loew, G. H.; Kirchner, R. F.; Mueller-Westerhoff, U. T. *J. Am. Chem. Soc.* **1980**, *102*, 589.

(21) HyperChem Computational Chemistry, Part 2: Theory and Methods; Hypercube, Inc., Publication HC40-00-03-00.

(22) Shipman, L. L.; Norris, J. R.; Katz, J. J. *J. Phys. Chem.* **1976**, *80*, 877.

(23) Pearlstein, R. M. In *Chlorophylls*; Scheer, H., Ed.; CRC Press: Boca Raton, 1991; pp 1047−1078.

(24) Gurinovich, G. P.; Zenkevich, E. I.; Chirvony, V. S.; Gadonas, R.; Pelakauskas, A. *Exp. Tech. Phys.* **1989**, *37*, 335.

(25) Oksanen, J. A. I.; Zenkevich, E. I.; Knyukshto, V. N.; Pakalnis, S.; Hynninen, P. H.; Korppi-Tommola, J. E. I. *Biochim. Biophys. Acta* **1997**, *1321*, 165.

(26) Pakalnis, S., Oksanen, J. A. I.; Korppi-Tommola, J. Unpublished results.

(27) Pullerits, T.; Chachisvilis, M.; Sundström, V. *Photosynth. Res., Suppl. 1* **1995**, 39.

(28) Freer, A.; Prince, S.; Sauer, K., Papiz, M.; Hawthornthwaite-Lawless, A.; McDermott, G.; Gogdell, R.; Isaacs, N. W. *Structure* **1996**, *4*, 449.

(29) Fong, F. K; Koester, V. J. *J. Am. Chem. Soc.* **1975**, *97*, 6888.

(30) Katz, J. J. *Spectrum* **1994,** *7*, 1.

(31) Helenius, V. M.; Siikki, J. O.; Hynninen, P. H.; Korppi-Tommola, J. E. I. *Chem. Phys. Lett.* **1994**, *226*, 137.

(32) Katz, J. J.; Bowman, M. K., Michalski, T. J.; Worcester, D. L. In *Chlorophylls;* Scheer, H., Ed.; CRC Press: Boca Raton, FL, 1991; p 221.

(33) Shipman, L. L.; Cotton, T. M.; Norris, J. R.; Katz, J. J. *Proc. Natl. Acad. Sci. U.S.A.* **1976**, *73*, 1791.

(34) Fong, F. K. *Proc. Natl. Acad. Sci. U.S.A.* **1974**, *71*, 3692.

(35) Worcester, D. L.; Michalski, T. J.; Katz, J. J. *Proc. Natl. Acad. Sci. U.S.A.* **1986,** *83*, 3791.

(36) Olson, J. M *Biochim. Biophys. Acta* **1980**, *594*, 33.

(37) Holzwarth, A. R., Griebenow, K.; Schaffner, K. *J. Photochem. Photobiol. A* **1992**, *65*, 61.

(38) Hirota, M.; Tsuji, K.; Shimada, K.; Miller, M.; Olson, J. M.; Matsuura, K. *Biochim. Biophys. Acta* **1992**, *1099*, 271.

(39) Van Amerongen, H.; Vasmel, H.; Van Grondelle, R. *Biophys. J.* **1988**, *54*, 65.

(40) Fetizova, Z. G.; Mauring, K.; Taisova, A. S. *Photosynth. Res.* **1994**, *41*, 205.

(41) Psencik, J.; Vacha, M.; Adamec, F., Ambroz, M.; Dian, J.; Bocek J.; Hala, J. *Photosynth. Res.* **1994**, *42*, 1.